EFDA–JET–CP(14)02/07

A.E. Shumack, J. Rzadkiewicz, M. Chernyshova, K. Jakubowska, M. Scholz, A. Byszuk, R. Cieszewski, T. Czarski, W. Dominik, L. Karpinski, G. Kasprowicz, K. Pozniak, A. Wojenski, W. Zabolotny, N.J. Conway, S. Dalley, J. Figueiredo, T. Nakano, S. Tyrrell, K.-D. Zastrow, V. Zoita and JET EFDA contributors

X-Ray Crystal Spectrometer Upgrade for ITER-Like Wall Experiments at JET

X-Ray Crystal Spectrometer Upgrade for ITER-Like Wall Experiments at JET

A.E. Shumack[1,2], J. Rzadkiewicz[3], M. Chernyshova4, K. Jakubowska[4,5], M. Scholz[6], A. Byszuk[8], R. Cieszewski[8], T. Czarski[4], W. Dominik[7], L. Karpinski[4], G. Kasprowicz[8], K. Pozniak[8], A. Wojenski[8], W. Zabolotny[8], N.J. Conway[1], S. Dalley[1], J. Figueiredo[9,10], T. Nakano[11], S. Tyrrell[1], K.-D. Zastrow[1], V. Zoita[9] and JET EFDA contributors*

JET-EFDA, Culham Science Centre, OX14 3DB, Abingdon, UK

[1]EURATOM-CCFE Fusion Association, Culham Science Centre, OX14 3DB, Abingdon, OXON, UK
[2]FOM Institute DIFFER P.O. Box 1207 NL-3430 BE Nieuwegein, The Netherlands
[3]National Centre for Nuclear Research, Andrzeja Sołtana 7, 05-400 Otwock, Poland
[4]Institute of Plasma Physics and Laser Microfusion, Hery 23, 01-497 Warsaw, Poland
[5]Université Bordeaux, CNRS, CEA, CELIA, UMR 5107, F-33405 Talence, France
[6]Institute of Nuclear Physics PAN, ul. Radzikowskiego 152,31-342 Kraków, Poland
[7]Warsaw University, Faculty of Physics, Institute of Experimental Physics, 00-681 Warsaw, Poland
[8]Warsaw University of Technology, Institute of Electronic Systems, 00-665 Warsaw, Poland
[9]EFDA-CSU, Culham Science Centre, Abingdon, OX14 3DB, UK
[10]Associação EURATOM/IST, Instituto de Plasmas e Fusão Nuclear, Instituto Superior Técnico, Av Rovisco Pais, 1049-001 Lisbon, Portugal
[11]Japan Atomic Energy Agency, Naka, Japan
[12]The National Institute for Laser, Plasma and Radiation Physics, Association EURATOM-MEdC, Magurele-Bucharest, Romania
** See annex of F. Romanelli et al, "Overview of JET Results", (24th IAEA Fusion Energy Conference, San Diego, USA (2012)).*

Preprint of Paper to be submitted for publication in Proceedings of the
20th Topical Conference on High-Temperature Plasma Diagnostics, Atlanta, Georgia, USA
1st June 2014 – 5th June 2014

ABSTRACT

The high resolution X-Ray crystal spectrometer at the JET tokamak has been upgraded with the main goal of measuring the tungsten impurity concentration. This is important for understanding impurity accumulation in the plasma after installation of the JET ITER-like wall (main chamber: Be, divertor: W). This contribution provides details of the upgraded spectrometer with a focus on the aspects important for spectral analysis and plasma parameter calculation. In particular we describe the determination of the spectrometer sensitivity: important for impurity concentration determination.

1. INTRODUCTION

The plasma facing component materials in the international fusion experiment ITER, will be beryllium in the main chamber with tungsten (and tungsten coated) tiles in the divertor [1]. One of the goals of the ITER-like wall programme [2] at JET is to understand the effect of these facing components on the plasma performance. In order to diagnose the W concentration in the plasma, a high resolution X-Ray crystal spectrometer at JET has been upgraded to include an additional measurement channel. In parallel, the spectrometer's X-Ray detectors and data acquisition systems have also been upgraded. This contribution outlines the upgraded diagnostic with a focus on the aspects important for spectral analysis and determination of plasma parameters: rotation velocity, ion temperature and impurity concentration. In particular, we describe the spectrometer sensitivity determination. The detector and data acquisition system are covered in a separate paper [3].

2. SPECTROMETER DETAILS

The X-Ray spectrometer [4] (Fig.1) is in Johann configuration with a Rowland circle radius of R = 12.49m and two 20m long beam lines joined at a crystal chamber. The measurements are integrated over a line of sight that crosses the plasma beam twice, at a displacement of 20cm below the average magnetic axis of the discharge. The upgrade of the spectrometer involved the installation of a second measurement channel, new triple GEM [3, 5] (Gas Electron Multiplier) detectors and an upgraded data acquisition system [6, 7].

A second measurement channel was created by replacing the original germanium crystal with two smaller crystals, one above the other: SiO_2 (2d = 0.668nm) and Ge(220) (2d = 0.400nm), with dimensions: 230×35×5mm. The crystals are cylindrically bent in a bending jig to a radius of 24.98m and the beam line was divided in the vertical direction by a septum. Triple GEM detectors were installed at the end of the beam line for each measurement channel. The detectors are position sensitive (wavelength sensitive by virtue of the crystal dispersion), with 256 0.8mm wide measurement strips. The detectors are also energy sensitive at each position (via the pulse height spectrum). Using the pulse height spectrum, the accompanying fast digital data acquisition system separates the different orders of reflection of the crystal, a significant upgrade with respect to the previous diagnostic.

The two measurement channels are designed to measure respectively the W46+ M-shell line at around 5.2Å ($3p^5 3d^{10}$ 4d – $3p^6$ $3d^{10}$ transition) and the Ni^{26+} K-shell resonance line ($1s2p\ ^1P_1 - 1s^2\ ^1S_0$) at around 1.6Å. These lines are measured with the detector mounted at different positions on the Rowland circle (i.e. not simultaneously). Two L shell Mo^{32+} lines (~5.2Å) are also measured on the 'W channel'. Due to the size of the diagnostic, we are able to measure with a resolution of better than $\lambda/\Delta\lambda = 12000$ and 20000 and a linear dispersion of 0.10Å/m and 0.07Å/m, as calculated from spectrometer geometry for the SiO_2 and Ge(220) crystals respectively. The time resolution of the measurement is 10ms, but for average plasma temperatures integration over about 120ms is required to obtain sufficient statistics.

The entire spectral range of the spectrometer is shown in Fig.2 for the 'W channel' (1st order of reflection, 'W detector') and the 'Ni channel' (2nd order of reflection, 'Ni detector'). At each spectrometer position, the signal is twice as high for half of the spectrum. This effect is caused by the blocking of part of the line of sight by the inner wall of the vessel.

3. SENSITIVITY - PART-BY-PART CALCULATION

The sensitivity of a spectrometer can be expressed as $S = LT\eta$, where L is the luminosity [m^2sr], $L = R_i A_{cry} h_D / 2R$ [8], T the transmission of the beam line (dimensionless) and η the detector efficiency [cnts/ph]. For our spectrometer, the relevant values are crystal area $A_{cry} = 0.00805 m^2$, detector height $h_D = 0.09$m and Rowland circle radius R = 12.49m. The detector efficiency η [c/ph] is presented in Ref. 5. The values for the luminosity are adjusted for the vignetting due to the Be window in the non-diffracting direction, a factor of 0.94. The crystal integrated reflectivity R_i, calculations are presented below.

The beam line transmission T is determined by the windows in the evacuated beam line: a 300 μm Be window with grid (transmission = 0.786) at the torus and a 12μm Mylar window with support frame (transmission = 0.88) at the end of the beam line. There is also a 9cm thick He buffer between the beam line and the detector for the 'W detector' and a 13cm air space for the 'Ni detector'. We assume there are no impurities in the He buffer. The detector windows (5μm and 12μm Mylar respectively with 0.2μm Al coating) are included in the detector efficiency. The crystal reflectivity is also treated separately.

3.1 REFLECTIVITY

The integrated reflectivity of the crystals was calculated by means of file-oriented codes implemented in X-ray OPtics utilities (XOP) [9]. The reflectivity was calculated in Bragg geometry, assuming perfect, cylindrically curved crystals, by means of the multi-lamellar method [10, 11, 12].

It is known that stresses and dislocations can increase a crystal's reflectivity by decreasing the efficiency of extinction [13]. In order to estimate an upper limit on our calculations, we calculated the reflectivity for an extreme model, a mosaic, flat crystal, for which attenuation is due only to absorption. Kinematic diffraction theory [13] was used. The calculations require input of line

broadening by the crystal. The influence of this broadening on the crystal reflectivity saturates at a certain value of the full width half maximum (FWHM) of the line. It was this value of the FWHM that was used for the calculations. More work is being done to calculate the broadening more accurately, but for the moment our mosaic calculation is accurate as an upper limit. The reflectivity is a smooth function of Bragg angle and the appropriate values for each crystal and for each of the three orders of reflection are given in Table I. The upper limits obtained from kinematic theory for mosaic flat crystals are respectively 1.66 and 4.70 times higher than the multi-lamellar calculations for the SiO_2 and Ge crystals.

3.2 RESULTS

AAll calculated values are shown in Table I. The results for the sensitivity for W and Ni measurement channels respectively are $1.6 \cdot 10^{-11}$ and $6.5 \cdot 10^{-11}$ cnts.ph^{-1}m^{2}sr. This gives tungsten and nickel concentrations in the range: 10^{-6}–10^{-4}. These values use the the most accurate results. Using the upper limit on the reflectivity from the mosaic calculations would increase the sensitivity by almost a factor of five for nickel measurements. Inclusion of experimentally determined line broadening for the mosaic calculations in the future will narrow this discrepancy further. Examples of resulting Ni concentrations are shown in Fig.3. tungsten and molybdenum concentrations [14] are currently being benchmarked against other diagnostics.

4. SENSITIVITY CHECK – CONTINUUM EMISSION

We also used an independent means of checking the spectrometer sensitivity. We defined a factor Q: measured, divided by calculated continuum emission intensity. The continuum emission calculation uses the IONEQ code [15] together with electron density and temperature profiles from high resolution Thomson Scattering projected onto the line of sight of the spectrometer. It includes both free-free and free-bound continuum radiation. It assumes that Be is the dominant impurity, the concentration of which is calculated from the effective charge of the plasma (Z_{eff}). The value of Z_{eff} is obtained from continuum emission measurements in the visible range. In Fig.4, Q is shown for several shots. It has an average value of about 0.8 which is consistent with a possible overestimation of the integrated crystal reflectivity by about 20% due to crystal imperfections and falls well within the error of the part-by-part sensitivity calculation.

CONCLUSIONS

The JET high resolution X-Ray crystal spectrometer has been upgraded to measure tungsten concentrations for ITER-like wall studies (in addition to nickel concentration, rotation velocity and ion temperature). Two measurement channels are now available, each with crystal order of reflection separation, which aids vignetting function and plasma parameter determination. The sensitivity of the spectrometer has been calculated and checked against continuum emission measurements.

ACKNOWLEDGEMENTS

This work was supported by EURATOM and carried out within the framework of the European Fusion Development Agreement. The views and opinions expressed herein do not necessarily reflect those of the European Commission.

REFERENCES

[1]. R.A. Pitts, A. Kukushkin, A. Loarte, A. Martin, M. Merola, C. E. Kessel, V. Komarov and M. Shimada, Physica Scripta, **T138**, 014001 (2009)

[2]. J. Paméla, G.F. Matthews, V. Philipps, R. Kamendje and JET-EFDA Contributors, Journal of Nuclear Materials, **363-365**, 1-11 (2007)

[3]. M. Chernyshova, T. Czarski, W. Dominik, K. Jakubowska, J. Rzadkiewicz, M. Scholz, K. Pozniak, G. Kasprowicz and W. Zabolotny, JINST, 9, C03003

[4]. R. Bartiromo, F. Bombarda, R. Giannella, S. Mantovani, L. Panaccione and G. Pizzicaroli, Review of Scientific Instruments, **60**, 237 (1989)

[5]. J. Rzadkiewicz, et al., Nuclear Instruments Methods in Physics Research A **36**, 720 (2013)

[6]. G. Kasprowicz, et al., Proceedings of the SPIE 8008 (2011) 80080J.

[7]. K. Pozniak, et al., Proceedings of the SPIE 8008 (2011) 800808.

[8]. R. Bartiromo, R. Giannella, M.L. Apicella, F. Bombarda, S. Mantovani and G. Pizzicaroli, Nuclear Instruments and Methods in Physics Research **225**, 378 (1984).

[9]. M. Sanchez del Rio, C. Ferrero and V. Mocella, Proc. SPIE, 3151, 312 (1997).

[10]. J.E. White, Journal of Applied Physics **21**, 855 (1950).

[11]. G. Egert and H. Dachs, Journal of Applied Crystallography **3**, 214 (1970).

[12]. A. Boeuf, S. Lagomarsino, S. Mazkedian, S. Melone, P. Puliti and F. Rustichelli, Journal of Applied Crystallography **11**, 442 (1978).

[13]. W. Zachariasen, Theory of X-ray diffraction in crystals (Dover, New York, 1967).

[14]. T. Nakano et al., to appear in Proceedings of the 41st EPS conference on plasma physics, 2014

[15]. A. Weller, D. Pasini, A.W. Edwards, R.D. Gill, R. Granetz, JET Joint Undertaking internal Report JET-IR-(87)10 (1987).

Crystal /Reflection order/Photon E [keV]	R_i [μrad]	Upper limit R_i [μrad]	T	η (c/ph)	L (m^2 sr) $.10^{-10}$	S (c ph^{-1} m^2 sr) $.10^{-10}$
SiO_2 / 1st/2.4	33.3	55.4	0.04	0.45	9.06	0.16
SiO_2 / 2nd/4.8	3.8	7.2	0.50	0.57	1.03	0.29
SiO_2 / 3rd/7.2	2.4	6.7	0.63	0.25	0.67	0.11
Ge / 1st/3.9	115	293	0.10	0.69	31.15	2.21
Ge / 2nd/7.8	21.9	103	0.55	0.20	5.96	0.65
Ge / 3rd/11.7	3.08	4.9	0.64	0.07	0.84	0.04

Table 1: Absolute sensitivity calculation S=LTη for the JET high resolution X-Ray crystal spectrometer. Parameter values relevant for W^{46+} and Ni^{26+} lines are highlighted.

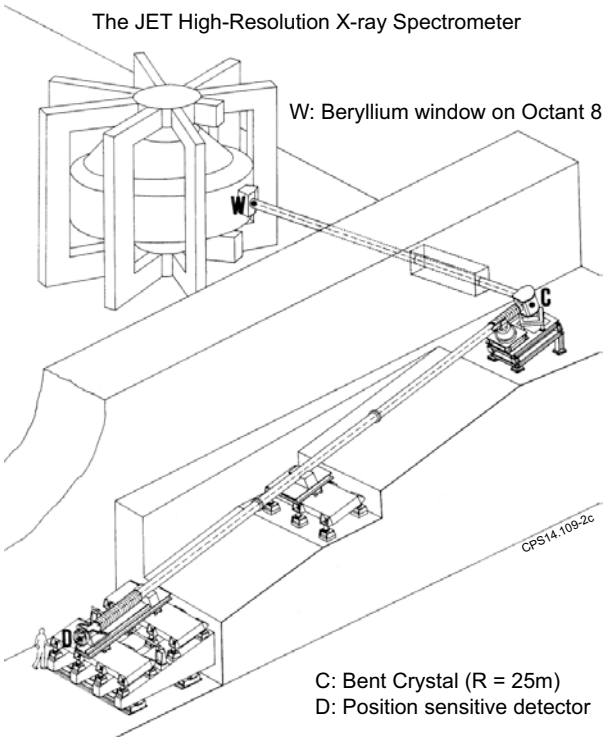

Figure 1: The JET high resolution X-Ray crystal spectrometer.

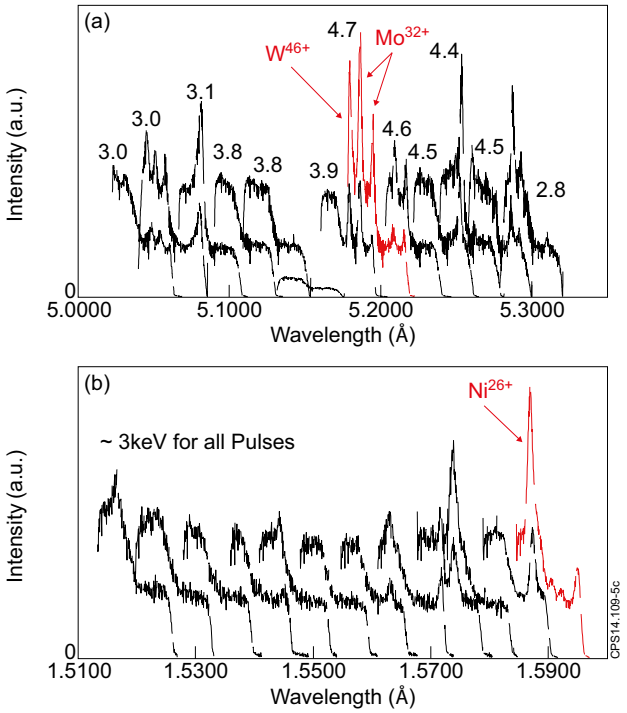

Figure 2: The entire spectral range of the spectrometer for the (a) 'W channel' (b) 'Ni channel'. Each trace corresponds to the integration over an entire plasma pulse at one spectrometer position. The numbers correspond to the peak electron temperature for the pulse, in keV. The highlighted trace is the standard position for measurements on each channel.

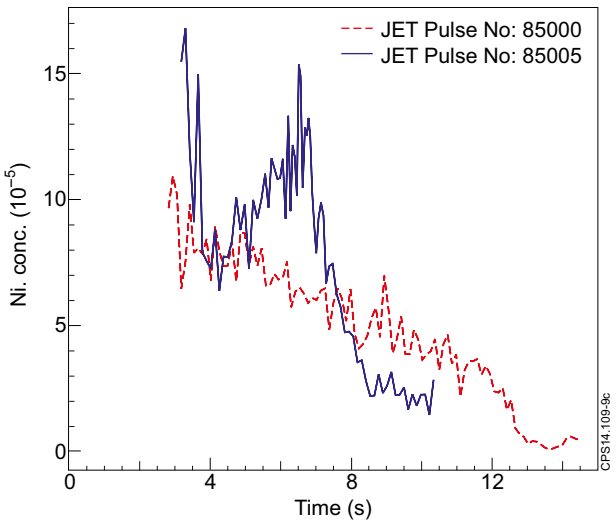

Figure 3: Examples of Ni concentrations.

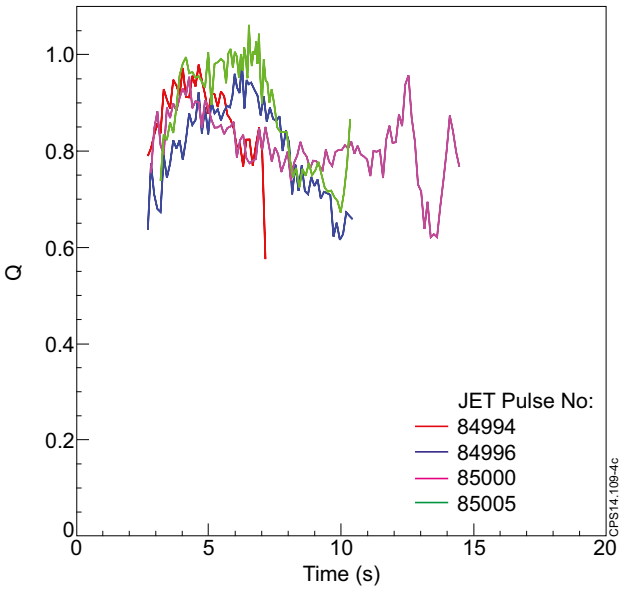

Figure 4: Ratio measured to calculated continuum as a check of the part - by - part sensitivity calculations (Q defined in text).